AGU Advances

RESEARCH ARTICLE
10.1029/2025AV002166

Peer Review The peer review history for this article is available as a PDF in the Supporting Information.

Key Points:

- Global analysis of decades of satellite data and flow records shows spatial configuration and kinematic changes along 97 multithread rivers
- Flow intermittency controls thread count, thread width, partitioning of discharge among threads, and bank migration rates
- Rivers with more threads build narrower channel belts but rework their channel-belt area more rapidly

Supporting Information:

Supporting Information may be found in the online version of this article.

Correspondence to:

F. Zhao,
xiafeizhao@ucsb.edu

Citation:

Zhao, F., Ganti, V., Chadwick, A., Greenberg, E., McLeod, J., Liu, Y., et al. (2026). Global hydroclimatic controls on multithread River dynamics. *AGU Advances*, *7*, e2025AV002166. https://doi.org/10.1029/2025AV002166

Received 16 OCT 2025
Accepted 9 FEB 2026

Author Contributions:

Conceptualization: Feifei Zhao, Vamsi Ganti
Data curation: Feifei Zhao, Austin Chadwick, Evan Greenberg, Jonah McLeod, Yinxue Liu, Louise Slater
Formal analysis: Feifei Zhao, Vamsi Ganti
Funding acquisition: Vamsi Ganti, Efi Foufoula-Georgiou
Investigation: Feifei Zhao, Austin Chadwick, Evan Greenberg, Jonah McLeod, Yinxue Liu, Louise Slater, Efi Foufoula-Georgiou
Methodology: Feifei Zhao, Vamsi Ganti, Austin Chadwick, Evan Greenberg

Global Hydroclimatic Controls on Multithread River Dynamics

Feifei Zhao[1], Vamsi Ganti[1], Austin Chadwick[2], Evan Greenberg[3], Jonah McLeod[4], Yinxue Liu[5,6], Louise Slater[5], and Efi Foufoula-Georgiou[7]

[1]Department of Geography, University of California Santa Barbara, Santa Barbara, CA, USA, [2]Columbia Climate School, Columbia University in the City of New York, New York, NY, USA, [3]Jet Propulsion Laboratory, California Institute of Technology, Pasadena, CA, USA, [4]Department of Earth Science and Engineering, Imperial College London, London, UK, [5]School of Geography and the Environment, University of Oxford, Oxford, UK, [6]School of Architecture, Building and Civil Engineering, Loughborough University, Loughborough, UK, [7]Department of Civil and Environmental Engineering & Earth System Science, University of California Irvine, Irvine, CA, USA

Abstract Most large rivers in densely populated areas split flow into multiple channels, forming interconnected pathways called threads. Multithread rivers are sensitive to hydroclimatic changes, yet understanding their dynamics is challenging due to the lack of robust metrics to characterize their evolution. To investigate the drivers of river evolution, we analyze 38 years of Landsat imagery alongside discharge records for 97 multithread reaches worldwide spanning diverse climates and both wandering and braided morphologies. We quantify the number of active threads and their allocated discharge through space and time using the entropic Braiding Index (*eBI*), coupled with metrics for bank migration rate, floodplain reworking, and channel-belt size. Data reveal that multithread river dynamics are strongly controlled by flow intermittency—expressed as the dimensionless ratio of long-term mean discharge to bankfull discharge. Rivers with lower flow intermittency (i.e., higher discharge relative to bankfull conditions) exhibit more active threads, decelerated thread migration, prolonged floodplain reworking timescales, and smaller channel-belt area normalized by channelized area. Lower flow intermittency also results in preferential flow routing among threads (lower *eBI* relative to thread count). Channel-belt area relative to channelized area exponentially declines with thread count, potentially reflecting a greater propensity for reconfiguration over lateral migration in braided rivers. Furthermore, multithread rivers in cold climates exhibit slower evolution rates across scales likely due to permafrost influence. Together, results suggest that future increases in discharge variability could cause multithread rivers to split into more active threads and accelerate movement within channel belts, potentially impacting livelihoods and ecosystems along river corridors.

Plain Language Summary Earth's largest rivers typically split flow into many interconnected pathways, called threads. Multithread rivers change their planform shape in response to variations in water flow and sediment delivery. However, studying these rivers has been difficult due to limited long-term observations and analytical tools to accurately characterize their evolution. We analyzed 38 years of satellite images alongside river flow data from 97 multithread rivers worldwide. We found that increased dimensionless discharge values—defined as the ratio of long-term average discharge to bankfull capacity of a river to carry flow—are associated with an increase in the number of active threads, emergence of one or more threads that carry majority of flow, and a slowdown of river evolution. This result highlights that flow variability, when viewed through the lens of channel morphology, is the dominant control on multithread river dynamics. We also find that multithread rivers in cold climates evolve more slowly compared to their counterparts in other climate zones likely due to the influence of permafrost. With climate change increasing flow variability, we predict that multithread rivers will increase their thread count and become more dynamic globally, potentially impacting livelihoods and ecosystems in river corridors.

1. Introduction

Multithread rivers—river systems characterized by multiple interwoven flow pathways or threads separated by mid-channel bars—dominate many of Earth's largest and most populated basins (Best, 2019; Latrubesse, 2008; Leopold & Wolman, 1957). These dynamic rivers adjust their spatial configurations and movements in response to variations in water discharge and seasonal flooding (Ashmore et al., 2011). However, our understanding of the

Project administration: Feifei Zhao, Vamsi Ganti
Software: Feifei Zhao
Supervision: Vamsi Ganti
Validation: Feifei Zhao
Visualization: Feifei Zhao, Austin Chadwick
Writing – original draft: Feifei Zhao, Vamsi Ganti
Writing – review & editing: Feifei Zhao, Vamsi Ganti, Austin Chadwick, Evan Greenberg, Jonah McLeod, Yinxue Liu, Louise Slater, Efi Foufoula-Georgiou

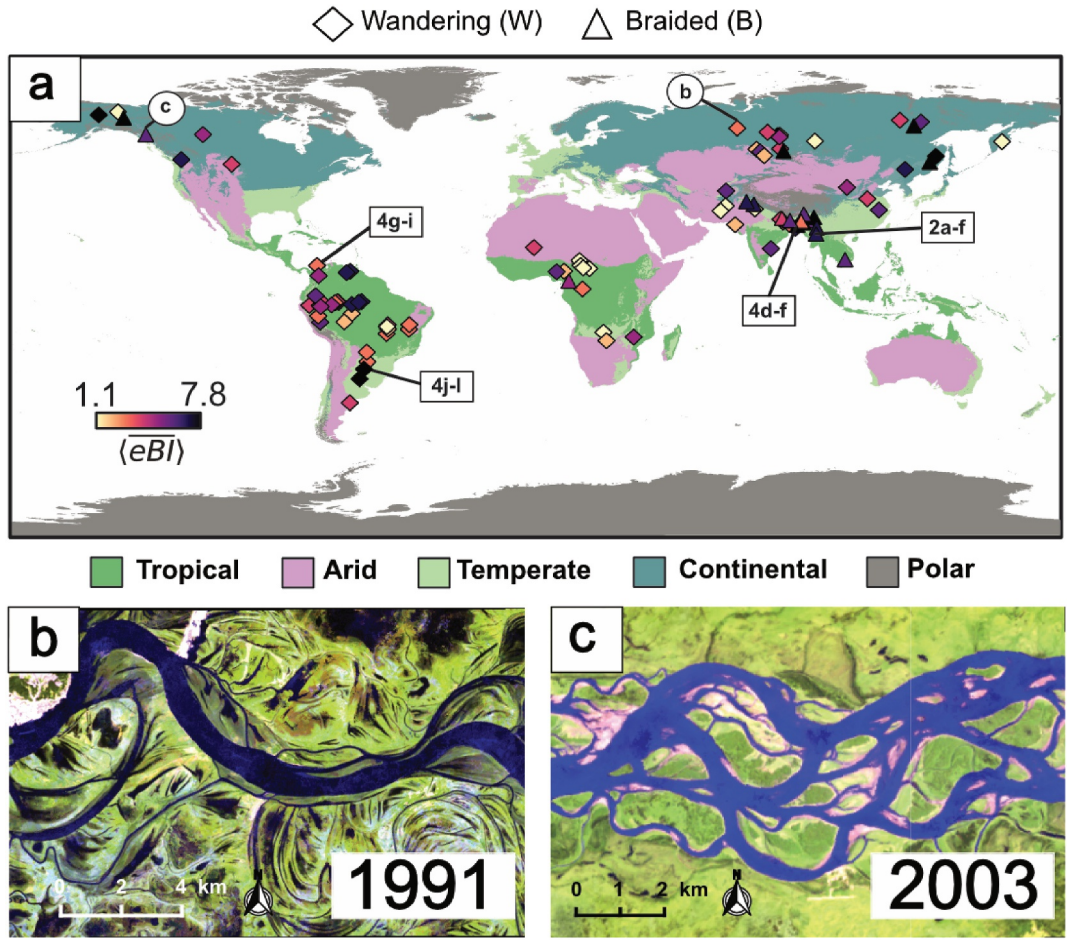

Figure 1. (a) Map of stream gauge locations and study reaches, overlaid on a Koppen-Geiger climate zone map (Kotteck et al., 2006). Marker shape denotes planform type, and marker color denotes the reach- and time-averaged entropic braiding index (*eBI*). Rectangular labels indicate reaches highlighted in other figures. Circles mark two example multithread reaches shown in Landsat images from (b) the Irtysh River (wandering) and (c) the Yukon River (braided).

factors controlling multithread river evolution lags that of single-thread rivers, which have received considerably more attention (Constantine et al., 2014; Greenberg & Ganti, 2024; Hickin & Nanson, 1984; Ielpi & Lapôtre, 2020, 2022; Mason & Mohrig, 2019). This limited understanding stems partly from the inherent diversity of multithread river planforms, commonly classified as wandering, anabranching, braided, or anastomosing (e.g., Carling et al., 2014; Eaton et al., 2010; Galeazzi et al., 2021; Leopold & Wolman, 1957) (Figure 1). Current classifications often rely on qualitative assessments and single snapshots of multithread river morphology, lacking a dynamic quantitative framework (Carling et al., 2014; Ethridge, 2011; Miall, 2014).

Despite being commonly classified using static planform metrics, multithread rivers are inherently dynamic systems that actively reconfigure individual threads (Eaton et al., 2010; Huang & Nanson, 2007; Leopold & Wolman, 1957). Like single-thread rivers, they migrate laterally (Chadwick et al., 2025) and undergo avulsions—periodic abrupt shifts in river course (Brooke et al., 2022; Slingerland & Smith, 2004; Valenza et al., 2020)—constructing channel belts over millennial timescales. The channel-belt geometry serves as a geological archive, preserving evidence of geomorphic work performed by rivers over millennia (Bridge, 1985; Dong & Goudge, 2022; Miall, 1994; Nyberg et al., 2023). Recent work suggests that increasing thread count accelerates floodplain reworking (Greenberg et al., 2024) but often results in narrower channel belts relative to total river width (Dong & Goudge, 2022; Greenberg et al., 2024). The evolution of these rivers may pose immediate risks to riverside communities (Church & Ferguson, 2015; Thakur et al., 2012) and exerts long-term control on terrestrial sediment and carbon cycling (Geyman et al., 2025; Repasch et al., 2021; Torres et al., 2017). However, we lack an understanding of the factors governing spatial and kinematic adjustments in multithread rivers. Analyzing lateral

migration in these complex geometries remains challenging due to limited analytical tools specifically designed for them (Chadwick et al., 2023). This knowledge gap is particularly critical because rivers are increasingly subject to altered runoff patterns, flood regimes, and sediment supply due to climate and land-use changes (Dethier et al., 2022; Immerzeel et al., 2010; Li et al., 2021). With over 3 billion people living along river corridors worldwide (Best, 2019), predicting the evolution of multithread rivers is increasingly urgent.

Previous studies have employed numerical models, physical experiments, and field observations to study multithread river evolution (Bertoldi et al., 2008; Egozi & Ashmore, 2008; Howard, 1996; Limaye, 2020; Mosley, 1983; Sapozhnikov & Foufoula-Georgiou, 1997; Sapozhnikov et al., 1998; Zhao et al., 2024). Researchers frequently use the braiding index (*BI*) to quantify river complexity, calculating the spatially averaged number of threads per river cross-section (e.g., Egozi & Ashmore, 2009; Kleinhans & van den Berg, 2011; Limaye, 2017; Limaye et al., 2018; Nicholas, 2013). Experiments demonstrate that increased water discharge and sediment supply can increase *BI* (Ashmore, 2009; Egozi & Ashmore, 2009; Jerolmack, 2009). However, *BI* does not capture well the diversity of flow division in multithread rivers—some rivers evenly distribute flow among threads, while others show a preference for a subset of large primary threads with smaller secondary threads (Tejedor et al., 2022). The response of this thread diversity to changing discharge remains unclear. Furthermore, experimental predictions of increased *BI* with higher water discharge require validation with decadal-scale observations from natural rivers, which are essential for understanding river responses to long-term climate and hydrologic forcings.

Today, nearly four-decades of global satellite imagery and river gauge station measurements offer an unprecedented opportunity to characterize multithread river dynamics. Recent advances in remote sensing and analytical techniques enable us to quantify the number, diversity, and relative sizes of active threads in multithread rivers (Tejedor et al., 2022), precisely measure riverbank migration rates for individual threads (Chadwick et al., 2023, 2025), characterize reach-scale floodplain reworking timescales (Greenberg et al., 2023, 2024), and identify channel-belt footprints revealing long-term geomorphic activity (Dong & Goudge, 2022; Nyberg et al., 2023). These advancements collectively offer the potential to significantly improve our understanding of how multithread rivers reorganize over decadal and longer timescales.

Here, we leverage these recent advances to present a global characterization of multithread river evolution, analyzing 97 river reaches across diverse climate zones (Figure 1). We integrate large-scale datasets—including time series of water discharge, river planform evolution, estimates of bankfull discharge, and channel and channel-belt morphometry—and apply state-of-the-art methods to quantify the hydroclimatic drivers of multithread river dynamics. As detailed below, our work provides a comprehensive, global perspective on the dynamic evolution of multithread rivers, establishing a crucial baseline for predicting their response to changing hydroclimatic regimes driven by climate change and human activity.

2. Materials and Methods

We investigated the temporal evolution of 97 multithread river reaches (Section 2.1) by constructing time series of channel masks from Landsat imagery (Section 2.2). We used the native multispectral resolution of Landsat (30 m), without panchromatic sharpening. For each reach, we quantified thread configuration using the entropic braiding index (*eBI*; Tejedor et al., 2022; Section 2.3); measured channel movement using particle image velocimetry (Section 2.4; Chadwick et al., 2023, 2025) and determined the floodplain-reworking timescales (Section 2.5; Greenberg et al., 2023, 2024). We also quantified channel-belt size using topographic analysis and estimates of long-term wetted area from satellite imagery (Section 2.6; Dong & Goudge, 2022). Finally, we integrated these observations with monthly water discharge data, estimates of bankfull discharge, and river morphometry (Section 2.7) to evaluate the factors controlling the spatial configuration and kinematic evolution of multithread rivers. For any given reach, *eBI*, riverbank migration rates, and water discharge are time-varying variables, whereas floodplain reworking timescales, bankfull discharge, and channel and channel-belt morphometry are time-averaged variables.

2.1. Global Selection of Multithread River Reaches

We selected 97 multithread river reaches from a larger data set of 361 reaches compiled by Galeazzi et al. (2021), representing the full spectrum of channel patterns globally. Galeazzi et al. (2021) classified these reaches using average thread count and sinuosity—calculated as the ratio of reach length to the shortest path length—both

measured from single, high-resolution Planet images (5-m/pixel resolution). They defined braided rivers as having a thread count ≥3.5 and sinuosity ≤1.4, wandering rivers with a thread count between 1.4 and 3.5, and meandering rivers with sinuosity >1.4 and thread count <1.4. For our analysis, we focused on rivers with individual thread widths >150 m to ensure that each thread is resolved by multiple pixels, limiting relative photogrammetric uncertainty to ≤20%. We also excluded meandering rivers to focus solely on multithread rivers. This process yielded 97 multithread rivers spanning temperate, arid, tropical, and cold climate zones (Figure 1a), with $n = 18$ braided and $n = 79$ wandering rivers. We analyzed braided and wandering rivers separately to evaluate if their dynamics differed.

These 97 selected reaches exhibit a broad range of mean water discharge, bed slope, and bankfull width, providing a representative global sample of multithread rivers. Mean monthly water discharge (Q_{mean}) ranges from 17 to 170,642 m^3/s, riverbed slope (S) varies from 1×10^{-5} to 2.22×10^{-3}, and total wetted widths—defined as the summed wetted width of all active threads within a reach—range from 116.2 to 5292.7 m (data derived from Galeazzi et al., 2021).

2.2. Generating Channel Mask Time Series From Satellite Data

For each river reach, we defined a study area extending beyond the apparent channel belt in cross-stream width and at least 50 wetted widths downstream (Figures 2a–2c). This ensured coverage of natural spatial variations associated with threads, bars, and bends (Egozi & Ashmore, 2008). We visually confirmed that each reach maintained consistent geometry and a linear downstream increase in drainage area along its course. We then accessed 38 years (1985–2023) of atmospherically corrected surface reflectance data from Landsat imagery (Landsat 5 TM, 7 ETM+, and 8 OLI/TIRS) through Google Earth Engine (Gorelick et al., 2017). We generated binary surface water masks from multispectral data using the USGS Dynamic Surface Water Extent (DSWE) methodology (Jones, 2019), applying it to annual median composite images (Figure 2d). We used medium-confidence water classification from DSWE and filtered out lakes, wetlands, and other unchannelized water bodies based on their connectivity to the main channel using the Rivgraph tool (Schwenk & Hariharan, 2021). Employing median annual composites minimized the influence of sub-annual water extent fluctuations caused by water-level changes—a technique successfully used in previous studies tracking multithread river evolution (Chadwick et al., 2023, 2025; Greenberg et al., 2024; Leenman et al., 2025). This process produced time series of channel masks for all study reaches.

2.3. Quantifying Spatial Configuration of Multithread Rivers

For each river reach, we quantified spatial configuration using two indices: the traditional braiding index (*BI*) and the entropic braiding index (*eBI*). We evaluated these indices at both cross-sectional and reach scales. First, we used the Python package Rivgraph (Schwenk et al., 2020; Schwenk & Hariharan, 2021) to automatically define the river centerline and generate transects from binary channel masks (Figure 2d). Following Egozi and Ashmore (2008), we created at least 10 equally spaced cross-sections perpendicular to the river centerline (Figure 2d). At each cross-section, we calculated *BI* as the active thread count. We also computed *eBI*, which accounts for the distribution of thread sizes, using the following equation (Tejedor et al., 2022):

$$eBI = 2^H \tag{1}$$

where H is the Shannon entropy, calculated as:

$$H = -\sum_{i=1}^{BI} \frac{b_i}{B} \log_2 \frac{b_i}{B} \tag{2}$$

In Equation 2, b_i represents individual thread width and B is the total wetted river width at a given cross-section. Thread width has been widely shown to scale with water discharge in both rivers and deltas (e.g., Dong et al., 2020; Tejedor et al., 2022; Wang & Smith, 2025); therefore, *eBI* reflects how flow is routed through active threads. Rivers concentrating flow in one dominant thread will exhibit low *eBI* values regardless of measured *BI*, while rivers distributing flow equally among multiple threads will have high *eBI* values approaching *BI* when all threads possess equal width—indicating even partitioning of water discharge (Figure 3). We further computed the

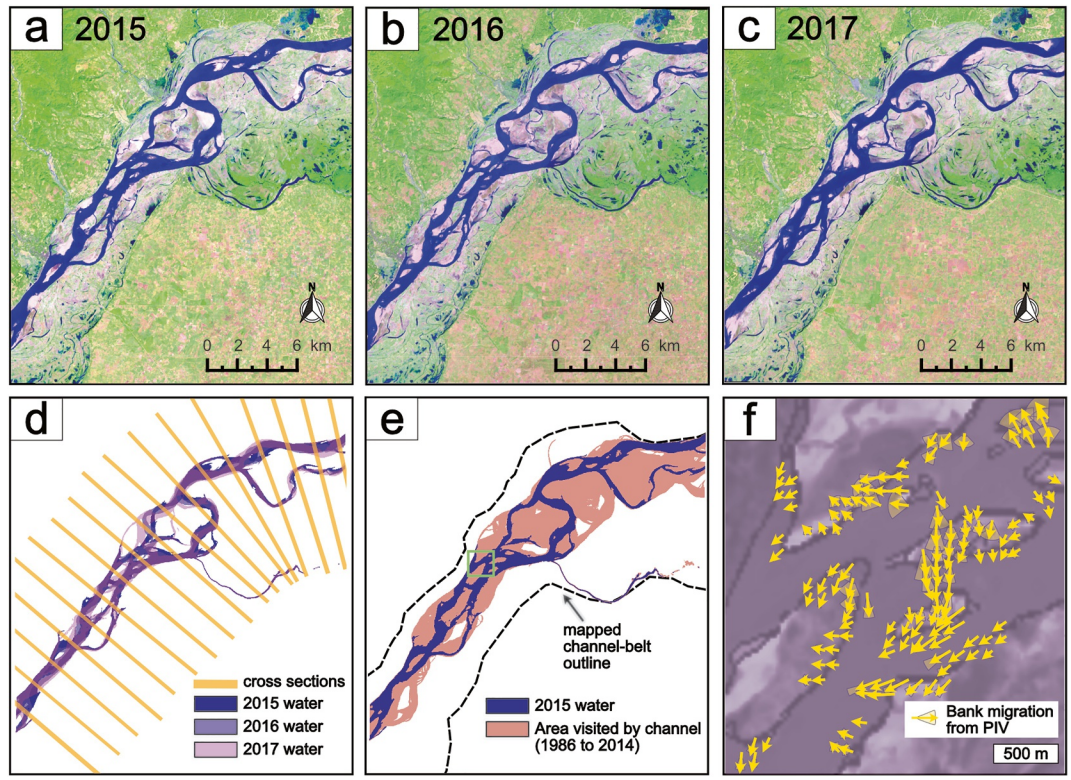

Figure 2. (a–c) Median annual composite Landsat images (SWIR1-NIR-Green) of the Irrawaddy River, Myanmar, for 2015, 2016, and 2017, respectively (see Section 2.2). (d) Calculation of the braiding index (*BI*) and the entropic braiding index (*eBI*) averaged across transects perpendicular to the river centerline, derived from Landsat water masks (2015–2017; see Section 2.3). (e) Computation of floodplain reworking area (pink area) from 1986 to 2014 used to estimate the floodplain reworking timescale, T_R (see Section 2.5). Green box denotes zoomed in window for (f) PIV-derived migration vectors for 2015–2016 (see Section 2.4).

ratio *eBI/BI* to assess flow partitioning among threads. A ratio near one indicates even distribution (i.e., no preferential thread), while a lower ratio suggests preferential routing through one or few threads (Figure 3).

We calculated *BI*, *eBI*, and *eBI/BI* at each sampled cross-section and timestep; so, these are time-varying, cross-section-scale variables for each river. We then averaged distributions across all cross sections within each reach to produce a reach-averaged time-series (denoted by an overbar, e.g., $\overline{eBI}$; this is also a time-varying variable for a river), as well as a single value representing the 38-year spatiotemporal mean (further denoted by angled brackets, e.g., $\langle \overline{eBI} \rangle$; a single, time-averaged value for a river).

2.4. Quantifying Riverbank Migration Rates of Individual Threads

We mapped riverbank migration rates using particle image velocimetry (PIV). Building on laboratory techniques, Chadwick et al. (2023, 2025) adapted PIV for global remote sensing of riverbank migration, demonstrating its ability to isolate bank migration from other mobility processes like cutoffs and avulsions, and its applicability across all channel patterns. Compared to traditional remote-sensing approaches to measuring river mobility (e.g., centerline-tracking using dynamic time warping; Sylvester et al., 2019), the PIV approach is well-suited for application to multithread rivers because PIV tracks individual banks in a Eulerian framework and propagates uncertainties in bank position (see Chadwick et al., 2023). Here, we utilized migration rates derived by Chadwick et al. (2025) for our study reaches. They applied PIV to Landsat images that are separated by an optimum timestep —determined by each river's mobility (Figure 2f)—and divided each image into a grid of interrogation windows. Within each window, cross-correlation analysis calculated displacement vectors capturing both the magnitude and direction of riverbank migration between timesteps. We then derived migration rates by dividing the magnitude of these vectors by the time interval and spatially averaged them to obtain a representative migration rate for each reach ($\overline{v}$).

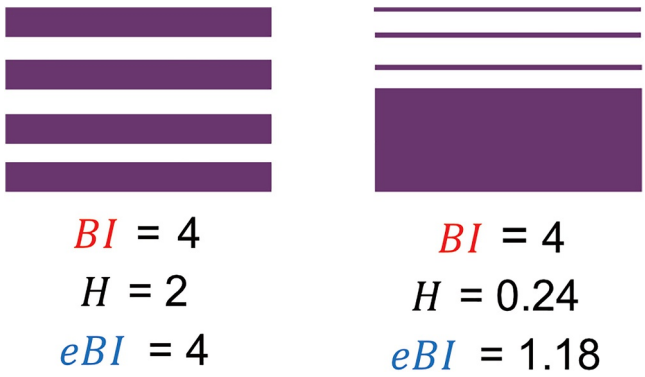

Figure 3. Schematic illustration showing two hypothetical multithread river configurations, where line width scales with thread width. This schematic highlights the difference between the braiding index (*BI*) and the entropic braiding index (*eBI*). While $BI = 4$ for both configurations, the value of Shannon entropy (H) is smaller for the configuration on the right, yielding a smaller *eBI*. The ratio *eBI/BI* quantifies preferential flow routing: values near 1 indicate even flow partitioning while lower values indicate dominance by one or several threads.

Of our 97 study sites, we obtained migration rates for 49 reaches (8 braided and 41 wandering reaches) as the method requires individual threads to be wider than 240 m and migrate at speeds conducive to reliable results (Chadwick et al., 2023). The timesteps used to measure migration rates varied from 1 to 8 years across these 49 reaches. Following previous work on single-thread rivers (Hickin & Nanson, 1984; Hooke, 2003), we calculated a normalized migration rate, $\overline{v^*}$, by dividing $\overline{v}$ by the average thread width. We refer the reader to Chadwick et al. (2023) for details of the PIV method, and Chadwick et al. (2025) for its application to our study sites.

2.5. Quantifying Multithread River Mobility

We quantified decadal-scale river mobility using a floodplain reworking timescale (T_R), derived from an area-based mobility framework (Greenberg et al., 2023). This method tracks the cumulative area of unchannelized pixels that transition to channelized over time, using the channel mask time series (Section 2.2). We normalized this cumulative area by the time-averaged channelized area (over 38 years of the satellite data) for each reach and monitored its growth. Each image in the time series served as a baseline for computing subsequent floodplain reworking, providing a time- and reach-integrated measure of river mobility. Greenberg et al. (2023) demonstrated that the growth in normalized cumulative reworked area with duration follows an exponential function; they defined T_R as a linear extrapolation of this growth, representing the minimum time required for the channel to rework a floodplain area equal to its time-averaged channelized area (Figure 2e). This definition ensures T_R is scale-independent—overcoming limitations of other vector-based methods dependent on timescales—and applies equally to all channel patterns. Importantly, this approach integrates all mobility processes, offering a process-integrated view of the kinematic evolution of multithread rivers that complements the PIV analysis (Section 2.4). We estimated T_R for all 97 reaches, with 47 estimates previously reported in Greenberg et al. (2024). We refer the reader to Greenberg et al. (2023, 2024) for a comprehensive review of the area-based mobility framework.

2.6. Quantifying Channel-Belt Size

Rivers construct channel belts through migration and avulsion, processes typically unfolding over millennial timescales. Recent advances in remote sensing allow us to delineate channel belts in plan view (Dong & Goudge, 2022; Nyberg et al., 2023), offering a long-term perspective on river mobility that is not captured by time series of satellite imagery alone. For each river reach, we mapped channel-belt boundaries following the method of Dong and Goudge (2022). Using NASADEM 30 m elevation data (NASA JPL, 2020) and the median annual Landsat composite image from 2000, we identified these boundaries using elevation differences marked by fluvial terraces and other topographic features, as well as sharp vegetation changes that suggest hydrologically driven successional changes (Salo et al., 1986). We then estimated the area between these boundaries and normalized it with the time-averaged channelized area, yielding the normalized channel-belt size, CB^*. This measure differs from the normalized channel-belt width of Dong and Goudge (2022), which normalized belt width by wetted channel width at the cross-section level. However, applying the Dong and Goudge (2022) method across a sufficiently large number of transects and averaging over a reach yields value comparable to CB^* metric.

2.7. Quantifying Hydroclimatic Variables Controlling Multithread River Dynamics

We investigated the hydroclimatic controls on the spatial configuration and kinematic evolution of multithread rivers. We first classified the Koppen-Geiger climate zone that each reach belonged to and assessed if river dynamics varied across climate for similar river types. In addition, for each river reach, we compiled gauged monthly discharge data spanning 1–117 years from the Global Runoff Data Center (GRDC), and calculated the long-term average discharge, Q_{mean}. 36 of the 97 rivers had complete 38-year data sets coinciding with satellite observations. Recognizing that water discharge variability significantly influences river mobility (e.g., Hansford et al., 2020; Leenman et al., 2025; Slater & Singer, 2013), we also computed the coefficient of variation of discharge, Q_{cov}, defined as the ratio of the standard deviation and mean water discharge computed over the entire

discharge record. Additionally, following Limaye et al. (2018), we calculated a dimensionless water discharge by normalizing the mean water discharge by acceleration due to gravity (g) and the average thread width in a multithread river (Text S1 in Supporting Information S1):

$$Q^* = \frac{Q_{\text{mean}}\text{WDR}^{3/2}\langle \overline{BI} \rangle^{3/2}}{g^{\frac{1}{2}}B^{5/2}\left(\frac{S}{C_f}\right)^{1/2}} \tag{3}$$

where WDR is the bankfull width-to-depth ratio of individual threads (fixed at 20 consistent with experimental and field channels; Métivier et al., 2017; Zarrabi et al., 2025), B is the average wetted width over the duration of satellite imagery, $\langle \overline{BI} \rangle$ is the site-mean braiding index, S is channel slope, and C_f is a friction factor (assumed constant at 0.01, typical of alluvial rivers; Dunne & Jerolmack, 2018; see Text S1 in Supporting Information S1 for full derivation). Typically, the dimensionless discharge is calculated by normalizing mean discharge by median bed-material grain size (Métivier et al., 2017; Parker et al., 2007), which is difficult to estimate from remote sensing data. Instead, Limaye et al. (2018) used a bar size as representative length scale, which scales with the thread width in rivers (Greenberg et al., 2021).

Importantly, we observe that Q^* can be interpreted to represent flow intermittency, which is the ratio of the long-term average water discharge to bankfull river discharge (Text S1 in Supporting Information S1). Highly intermittent rivers with flashy flows should have $Q^* < 1$ and less intermittent, perennial rivers should have Q^* close to 1. A value of $Q^* \approx 1$ indicates that rivers transport water at bankfull conditions, on average. This metric is different from the simple coefficient of variation of discharge, as it views the flood variability through the lens of the channel, that is, rivers with similar Q_{cov} can have different Q^* values.

In addition to flow discharge variables, we evaluated how vegetation influences multithread river dynamics. Recent studies demonstrate that vegetation regulates the pace of single-thread river evolution (Greenberg & Ganti, 2024; Hasson et al., 2025; Ielpi & Lapôtre, 2020); however, comparable effects on multithread river evolution remain unestablished. We quantified vegetation extent within each river's channel belt using a satellite-derived vegetation index. For each river reach, we calculated the Normalized Difference Vegetation Index (NDVI) and defined vegetation extent as the fraction of channel-belt pixels with NDVI > 0.3, a threshold representing photosynthetically active vegetation (Tucker, 1979). To minimize sensitivity to interannual variability and data gaps, we estimated the vegetation extent as the median of values from the three most recent valid years for each river. We computed this vegetation metric independently and used it for comparative analysis across climate zones.

2.8. Relative Importance of Controls on Spatial Configuration and Kinematics

To identify and quantify the primary controls on spatial configuration and kinematic evolution of multithread rivers, we employed a random forest regression model alongside our analysis of hydroclimatic variables (Section 2.7). We used predictors including dimensionless water discharge, coefficient of variation of discharge, riverbed slope, $\langle \overline{eBI} \rangle$, standard deviation of $\overline{eBI}$, and floodplain reworking timescale. Each observation in the model corresponds to a single river reach, using time-aggregated metrics to avoid introducing temporal autocorrelation from repeated measurements. We built separate random forest models for braided and wandering rivers to account for potentially different kinematics between these channel patterns. For each model, the data set was split into 70% training and 30% testing subsets, and model performance was assessed on the held-out test set using the coefficient of determination (R^2) and root-mean square error (RMSE). Feature importance was computed based on the mean decrease in impurity across trees in the trained model. The number of samples per model ranged from 8 to 18 braided rivers and 41 to 79 wandering rivers, depending on whether migration rates were available for the river reach.

3. Results

3.1. Descriptive Statistics of Spatial Configuration and Kinematic Evolution

We quantified variations in eBI and BI at the cross-sectional, reach-averaged and time-averaged scales for braided ($n = 18$) and wandering rivers ($n = 79$). We note that eBI (or BI) and $\overline{eBI}$ are time-varying quantities, whereas

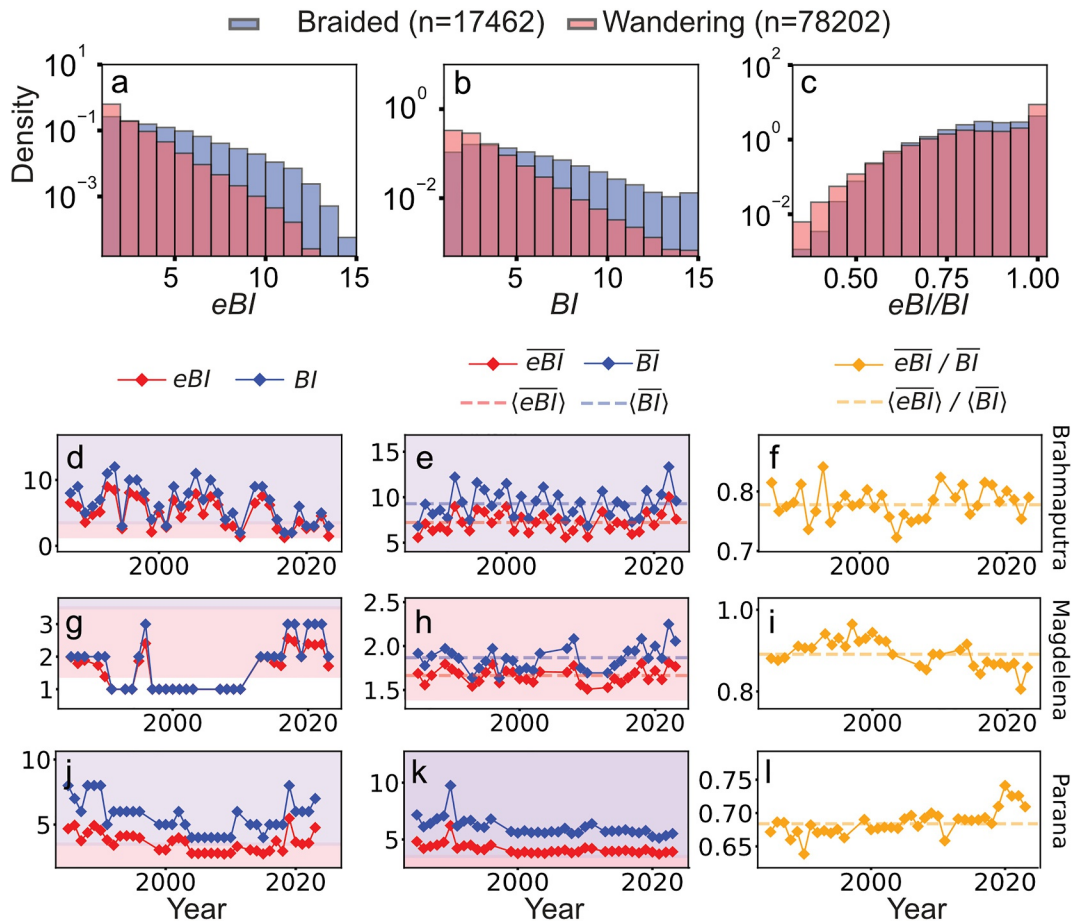

Figure 4. Histograms of cross-section-level (a) *eBI* (b) *BI*, and (c) *eBI/BI* across all rivers globally. Time series of (d) *eBI* and *BI* of the Brahmaputra River at a single cross section (the 10th cross section was chosen at random for each river), (e) after spatial averaging over the entire reach, and (f) the ratio of *eBI* and *BI* at the cross-section level. Dashed horizontal lines mark the reach and time-averaged values. Red and blue shaded areas indicate definitions of wandering (thread count <1.4) and braided reaches (thread count ≥3.5), respectively. Equivalent panels for the (g–i) Magdelena River, (j–l) the Parana River.

$\langle\overline{eBI}\rangle$ is a time-averaged quantity for each river. Braided rivers worldwide exhibited a mean cross-section-level *eBI* of 3.95 (median = 3.3; standard deviation (s.d.) = 2.12; n = 17,702; Figures 4a and 4d). Reach-averaged *eBI* ($\overline{eBI}$) values were similar (mean = 3.95; s.d. = 2.0), and reach- and time-averaged *eBI* (denoted as $\langle\overline{eBI}\rangle$) had mean of 4.04 (median = 3.5; s.d. = 2.6; Figure 4e). The mean and median $\langle\overline{BI}\rangle$ for braided rivers were 4.94 and 4.0, respectively (Figure 4b). The ratio eBI/BI averaged 0.86 ± 0.09 (mean ± s.d.) at the cross-sectional level, and 0.86 ± 0.11 when aggregated over reach and time (Figure 4c), indicating that ~86% of the threads effectively carry discharge while 14% carry only minor flow globally.

Wandering rivers exhibited lower $\langle\overline{eBI}\rangle$ (mean = 2.14; median = 1.89; s.d. = 1.34; Figure 4a) and $\langle\overline{BI}\rangle$ (mean = 2.56; s.d. = 1.9 for $\langle\overline{BI}\rangle$; Figures 4a, 4h, and 4k). Across all wandering reaches, cross-sectional estimates of *eBI* yielded a mean of 2.07 and s.d. of 1.06 (n = 78,296). The cross-section-level eBI/BI averaged 0.88 ± 0.10, and 0.89 ± 0.13 when aggregated over time and reach (Figure 4c). These results suggest that flow partitioning between threads is comparable in both wandering and braided rivers, despite differences in total thread counts.

Our PIV analysis showed that the median riverbank migration rates, $\bar{v}$, was 35.5 m/yr for braided rivers and 11 m/yr for wandering rivers. Normalized migration rates ($\overline{v^*}$) differed between the two channel patterns (P = 0.052; two-sample t-test; Text S2 in Supporting Information S1), averaging 0.08 ± 0.06 1/yr for braided rivers versus 0.03 ± 0.03 1/yr for wandering rivers. Consistent with faster normalized riverbank migration, floodplain reworking timescales were shorter in braided rivers (median T_R = 9.9 years) compared to

wandering rivers (median T_R = 53.8 years) ($P < 10^{-3}$ from two-sample t-test). The 5th–95th percentiles of T_R ranged from [4, 122] yr for braided rivers and [5, 231] yr for wandering rivers. However, braided rivers developed smaller normalized channel-belt areas (average of 5.4 ± 2.3) compared to wandering rivers (10.1 ± 6.4) ($P < 10^{-3}$; two-sample t-test), a result consistent with previous observations in smaller data sets (Dong & Goudge, 2022; Greenberg et al., 2024). We discuss the controls on this difference in Section 3.4.

Both braided and wandering rivers covered a comparable range of flow conditions. Mean water discharge, Q_{mean}, spanned a minimum-maximum range of [8, 2.2 × 10^4] m^3/s (median of 2495.3) for braided rivers and [5.5, 1.22 × 10^5] m^3/s (median of 2338 m^3/s) for wandering rivers. Dimensionless water discharge, Q^*, spanned a minimum-maximum range of [0.006, 0.604] and [0.013, 6.016] for braided and wandering rivers, respectively. Flow variability, as measured by Q_{cov}, spanned a minimum-maximum range of [0.79, 1.32] for braided rivers and [0.20, 1.82] for wandering rivers.

3.2. Controls on Spatial Configuration

Our results reveal significant differences in spatial configuration of multithread rivers across climate zones ($P = 0.007$; Kruskal-Wallis test; Text S2 in Supporting Information S1): temperate rivers exhibit the highest mean $\langle \overline{eBI} \rangle$ of 3.22, while arid rivers exhibit the lowest $\langle \overline{eBI} \rangle$ (1.82; Figure 1a). While the greatest variation in $\langle \overline{eBI} \rangle$ occurs within multithread rivers in temperate climates, this is partly influenced by a disproportionately high number of braided rivers in our temperate data set. Tropical rivers exhibit the highest temporal variability in $\overline{eBI}$, whereas cold-climate rivers exhibit the least. Results indicate significant differences in flow partitioning across climate zones ($P < 10^{-3}$; KW test): arid rivers distribute flow more evenly across threads (average $\langle \overline{eBI} \rangle / \langle \overline{BI} \rangle = 0.93$), while cold climate rivers preferentially route flow through one or few dominant threads (mean $\langle \overline{eBI} \rangle / \langle \overline{BI} \rangle = 0.85$). For most rivers, over 80% of threads carry majority of water discharge. Rivers exhibiting the most significant partitioning in our data set include the Amazonas ($\langle \overline{eBI} \rangle / \langle \overline{BI} \rangle = 0.63$), the Parana ($\langle \overline{eBI} \rangle / \langle \overline{BI} \rangle$, = 0.69) (Temperate; Figures 4i–4l), and the Solimoes river (Tropical; $\langle \overline{eBI} \rangle / \langle \overline{BI} \rangle = 0.71$).

We found that hydrological characteristics influence preferential flow partitioning, as measured by $\langle \overline{eBI} \rangle / \langle \overline{BI} \rangle$ (Figure 5). Both wandering and braided rivers exhibit a decrease in $\langle \overline{eBI} \rangle / \langle \overline{BI} \rangle$ with increasing mean water discharge (Spearman rank correlation coefficient $r = -0.67$, $P = 0.009$ for braided; $r = -0.74$, $P < 10^{-3}$ for wandering; Figure 5a), suggesting that preferential routing is more common in larger rivers of lowland regions (Figure 1a). Similarly, in the dimensionless framework, $\langle \overline{eBI} \rangle / \langle \overline{BI} \rangle$ decreases with dimensionless discharge (Q^*) at similar rates for both channel patterns ($r = -0.60$, $P = 0.009$ for braided; $r = -0.44$, $P < 10^{-3}$ for wandering), approaching unity at low Q^* values (Figure 5b). This observation indicates that flow intermittency exerts a control on the partitioning of flow between threads in a multithread river. However, the relationship between $\langle \overline{eBI} \rangle / \langle \overline{BI} \rangle$ and coefficient of variation of discharge (Q_{cov}) differs; we observe a positive correlation in wandering rivers ($r = 0.51$, $P < 10^{-3}$; Figure S2a in Supporting Information S1), suggesting greater discharge variability promotes more uniform flow partitioning, but no significant correlation exists for braided rivers ($r = 0.34$, $P = 0.16$; Figure S2a in Supporting Information S1).

Given the stronger spatial than temporal variability in eBI, we investigated hydrological factors controlling reach- and time-averaged entropic braiding index, $\langle \overline{eBI} \rangle$. We found that both braided and wandering rivers show a positive correlation between $\langle \overline{eBI} \rangle$ and Q_{mean} ($r = 0.83$; $P < 10^{-3}$ for braided; $r = 0.45$; $P < 10^{-3}$ for wandering). Power-law relationships further reveal that the increase in $\langle \overline{eBI} \rangle$ with Q_{mean} is more pronounced in braided rivers than wandering rivers (Figure 6a), a trend supported by previous experimental work (Bertoldi et al., 2009; Egozi & Ashmore, 2008). Notably, while these experiments focused on the effects of discharge variations on BI within individual reaches, our global data set indicates that this trend is consistent across diverse river reaches. We also find a positive correlation between $\langle \overline{eBI} \rangle$ and Q^*, with a sharper increase in braided rivers ($r = 0.34$, $P = 0.002$ for wandering; $r = 0.58$, $P = 0.01$ for braided; Figure 6b), indicating that rivers that carry water discharge at bankfull conditions, on average, are also characterized by a greater number of active threads. This covariance is also exemplified by Q^* being maximized in temperate and tropical rivers and being minimum in arid rivers, similar to $\langle \overline{eBI} \rangle$.

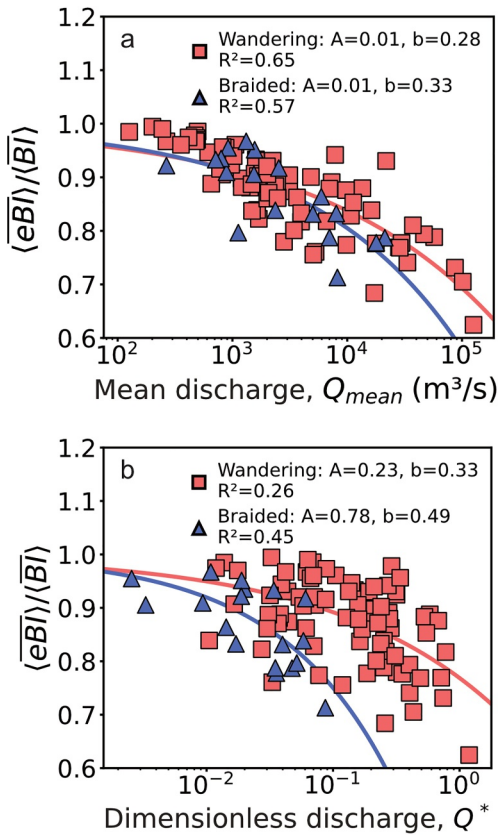

Figure 5. Functional dependence of the ratio of the entropic braiding index to braiding index on (a) mean water discharge and (b) dimensionless water discharge. In these parameter spaces, both wandering and braided rivers collapse on a similar trend. Blue triangles and red squares denote braided and wandering rivers, respectively. Both plots are on semi-log axes, with the fitted equation given by: $\langle\overline{eBI}\rangle/\langle\overline{BI}\rangle = 1 - Ax^b$. See Text S2 in Supporting Information S1 for details on fitted equations.

We further investigated factors influencing the temporal variability in *eBI* for each reach, quantified by the coefficient of variation of $\overline{eBI}$ through time, eBI_{cov} (Figure 7). We find no correlation between eBI_{cov} and Q^* for braided rivers and a positive correlation for wandering rivers ($r = 0.36$, $P = 0.001$ for wandering; $r = -0.46$, $P = 0.055$ for braided; Figure 7a). Interestingly, we observed a negative correlation between eBI_{cov} and Q_{cov}, only in wandering rivers ($r = -0.24$, $P = 0.03$ for wandering; $r = 0.42$, $P = 0.16$ for braided; Figure 7b). Finally, we found a negative correlation between Q_{cov} and $\langle\overline{eBI}\rangle$ (Figure 7c), with this trend being more pronounced in braided rivers ($r = -0.45$, $P = 0.06$) than wandering rivers ($r = -0.36$, $P = 0.001$).

Finally, we did not find any significant correlation between vegetation extent and $\langle\overline{eBI}\rangle$ and $\langle\overline{eBI}\rangle/\langle\overline{BI}\rangle$ (Figure S6 in Supporting Information S1). This result suggests that vegetation likely exerted a secondary effect on the spatial configuration of multithread rivers compared to flow discharge.

3.3. Controls on River Mobility and Channel-Belt Size

Our results demonstrate that river mobility varies across climate zones at bank ($\overline{v^*}$), reach (T_R), and millennial timescales (CB*). At the bank scale, we found the highest mean normalized migration rate ($\overline{v^*}$) in temperate climates (0.09), exceeding the lowest rates found in cold climates (0.01; Figure 8b). Similarly, floodplain reworking timescales (T_R) were shortest—indicating rapid river mobility—in temperate climates (Figure 8c). Normalized channel-belt area was largest in arid rivers, and smallest for rivers in cold climates (Figure 8d), suggesting that climate influences the pace of river mobility through differing hydrological controls. Across the bank, reach, and millennial timescales, one-way ANOVA tests confirmed that mean values differed significantly across climate zones ($P < 0.05$). Vegetation extent within the channel belt varies systematically with climate, with arid rivers exhibiting the lowest vegetation cover and tropical and temperate rivers exhibiting the highest (Figure S6 in Supporting Information S1). However, at comparable vegetation extent, $\overline{v^*}$ and T_R span broad and overlapping ranges across climate zones (Figure S6 in Supporting Information S1), indicating that vegetation extent alone does not exert a dominant control on multithread river mobility.

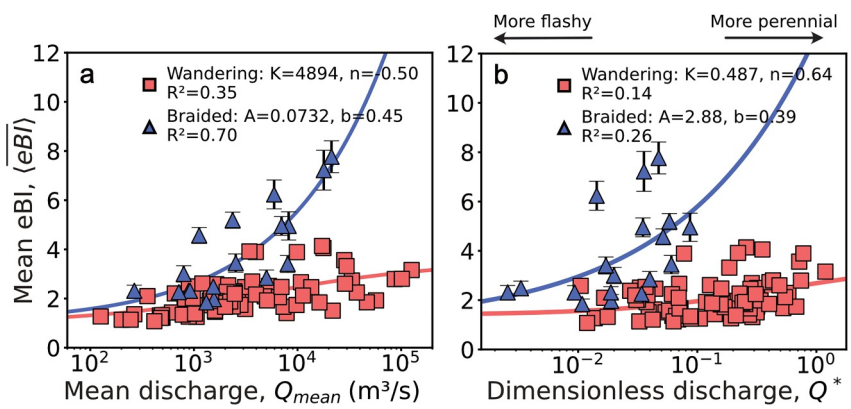

Figure 6. Functional dependence of time- and reach-averaged entropic braiding index on (a) mean water discharge and (b) dimensionless water discharge (Equation 3). Larger Q^* values indicate perennial flows while smaller Q^* values indicate more flashier flows. Blue triangles and red squares denote braided and wandering rivers, respectively. Data are shown on semi-log axes and the fitted equations for wandering and braided rivers are $\langle\overline{eBI}\rangle = 1.4 + 2.1/1 + \left(\frac{x}{k}\right)^n$ and $\langle\overline{eBI}\rangle = 3.5 + Ax^b$, respectively. See Text S2 in Supporting Information S1 for details on fitted equations.

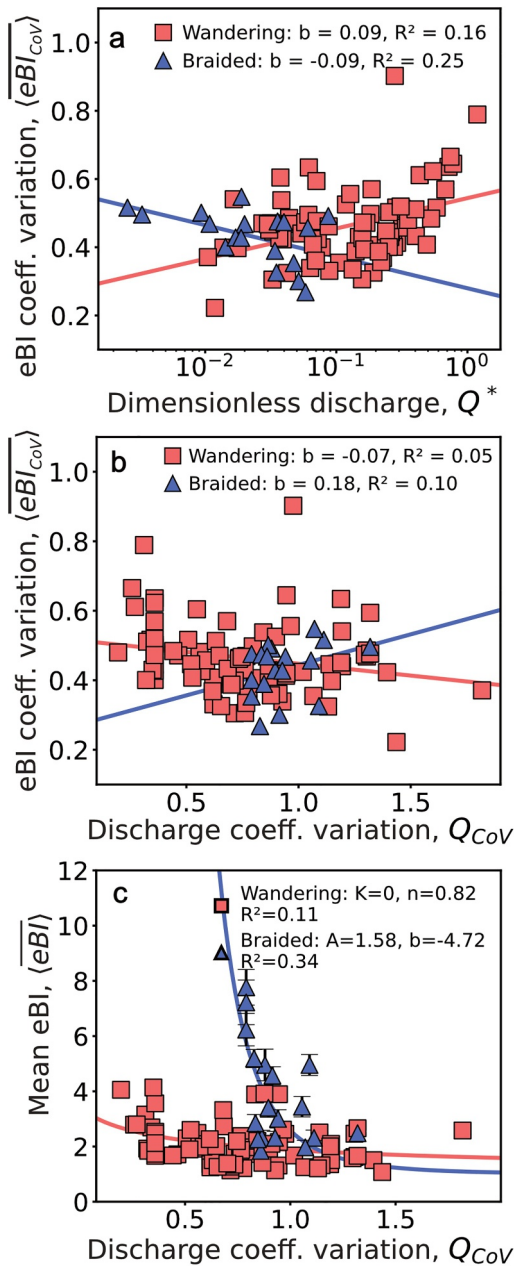

Figure 7. Functional dependence of the coefficient of variation of *eBI* through time on (a) dimensionless discharge (data shown on log-log axes) (b) coefficient of variation of water discharge. (c) Functional dependence of the reach- and time-averaged entropic braiding index of multithread rivers as a function of coefficient of variation of water discharge. Blue triangles and red squares denote braided and wandering rivers, respectively. Fitted equations for wandering and braided rivers in panel (c) are $\langle \overline{eBI} \rangle = 1.4 + 2.1/1 + \left(\frac{x}{K}\right)^n$ and $\langle \overline{eBI} \rangle = 3.5 + Ax^b$, respectively. The fitted equations in panels (a, b) are $y = a + b$*log x and $y = a + bx$, respectively. See Text S2 in Supporting Information S1 for details on fitted equations.

Examining bank-scale mobility, we found a positive correlation between Q_{mean} and migration rate only in braided rivers; wandering rivers showed no significant relationship ($r = 0.8$, $P = 0.02$ for braided; $r = -0.2$, $P = 0.2$ for wandering; Figure S2b in Supporting Information S1). While sample size for braided rivers is small ($n = 8$), this suggests that higher discharge directly drives faster migration in braided rivers. We observed a negative correlation between $\overline{v^*}$ and Q^* for both braided and wandering rivers, indicating that more ephemeral rivers exhibit higher migration rates, consistent with observations of faster lateral migration rates of meandering rivers in unvegetated environments (Ielpi & Lapôtre, 2020).

At the reach scale, T_R did not systematically vary with Q_{mean}, consistent with previous work (Leenman et al., 2025). However, T_R increased with Q^* following a power-law relationship for both wandering and braided rivers (Figure 9b), with similar exponents. T_R also decreased with flood discharge variability (Q_{cov}), aligning with findings from the subset of 47 overlapping reaches analyzed by Leenman et al. (2025), across both channel patterns.

At the belt scale, normalized channel-belt area was negatively correlated with Q_{mean} in wandering rivers but showed no significant correlation in braided rivers ($r = -0.33$, $P = 0.003$ for wandering; $r = -0.13$, $P = 0.62$ for braided; Figure S2c in Supporting Information S1). Normalized channel-belt area decreased with dimensionless discharge in braided rivers ($r = -0.08$, $P = 0.44$ for wandering; $r = -0.59$, $P = 0.009$ for braided; Figure 9c), exhibiting a faster growth in wandering than braided rivers (Figure 9c). The coefficient of variation of discharge ($r = 0.20$, $P = 0.07$ for wandering; $r = 0.35$, $P = 0.16$ for braided) was not significantly correlated with the normalized channel-belt area for either channel pattern (Figure S2d in Supporting Information S1).

3.4. Connections Between Spatial-Configuration Changes and River Mobility Across Scales

We investigated how spatial configuration, and its temporal changes, influenced river mobility across scales. At the bank scale, we found a weak negative power-law relation between $\langle \overline{eBI} \rangle$ and $\overline{v^*}$ in wandering rivers ($r = -0.28$, $P = 0.07$), but no such relation in braided rivers ($r = -0.28$, $P = 0.51$). We detected no association between $\overline{v^*}$ and temporal variation in *eBI* (quantified by eBI_{cov}) for either channel pattern ($r = 0.06$, $P = 0.70$ for wandering; $r = 0.19$, $P = 0.65$ for braided; Figure S2e in Supporting Information S1).

At the reach scale, we found no correlation between T_R and $\langle \overline{eBI} \rangle$ for either channel pattern ($r = 0.16$, $P = 0.17$ for wandering; $r = 0.20$, $P = 0.43$ for braided). However, eBI_{cov} correlated negatively with T_R only in braided rivers ($r = -0.66$, $P = 0.003$ for braided; $r = -0.07$, $P = 0.52$ for wandering; Figure 10a; Figure S2f in Supporting Information S1). This relationship followed a power law, indicating that faster reworking (shorter T_R) corresponds to greater spatial configuration changes (higher eBI_{cov}).

At the channel-belt scale, normalized channel-belt size decreased exponentially with $\langle \overline{eBI} \rangle$ (Figure 10b, Figure S3a in Supporting Information S1), consistent with previous studies (Dong & Goudge, 2022; Greenberg et al., 2024). Furthermore, eBI_{cov} positively correlated with normalized channel-belt area in braided rivers ($r = 0.50$, $P = 0.03$; Figure 10c), but not in wandering rivers ($r = -0.15$, $P = 0.20$).

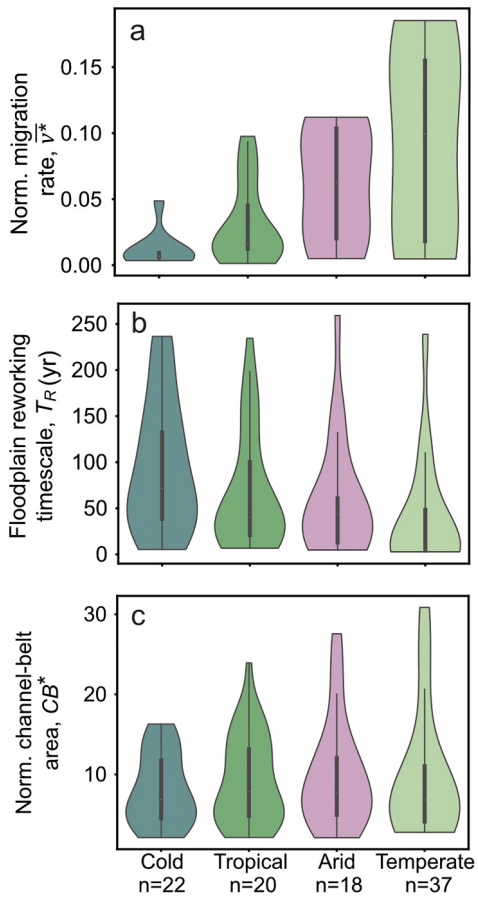

Figure 8. Violin plots of estimated (a) normalized riverbank migration rates, (b) floodplain reworking timescale, and (c) normalized channel-belt area as a function of climate zone. Each violin shows the kernel density distribution of values; the thick black bar indicates the interquartile range, and the thin line extends to the 10th–90th percentile range.

We observed that bank-scale river mobility relates to reach-scale river mobility in both channel patterns. We discovered a strong negative correlation ($r = -0.76$, $P = 0.03$ for braided; $r = -0.50$, $P = 0.001$ for wandering) between normalized migration rate and floodplain reworking timescale (Figure 10d), best described by a power-law function with similar exponents in both channel patterns. However, this faster pace of floodplain reworking associated with increasing normalized migration rate did not translate to changes in normalized channel-belt size ($r = 0.34$, $P = 0.41$ for braided; $r = 0.19$, $P = 0.24$ for wandering; Figure S3b in Supporting Information S1). We found a weak power-law dependence between normalized channel-belt area and normalized migration rates in multithread rivers (Figure S3b in Supporting Information S1). Finally, normalized channel-belt area showed a strong negative correlation with floodplain reworking timescale ($r = -0.37$, $P < 10^{-3}$ for wandering; $r = -0.46$, $P = 0.05$ for braided), indicating that normalized channel-belt size declines as T_R increases (Figure S3c in Supporting Information S1). The power-law exponents for this relationship were similar for both channel patterns, demonstrating that rivers reworking their floodplains faster also tend to build larger channel belts relative to their size.

3.5. Relative Controls on Spatial-Configuration and Kinematic Changes

Our random forest regression model reveals that dimensionless water discharge best predicts the number of active threads in wandering and braided rivers, followed by flow variability (quantified by Q_{cov}) and channel-bed slope ($R^2 = 0.7$; RMSE = 0.43; Figure 11a). The dimensionless discharge also strongly predicts $\langle \overline{eBI} \rangle / \langle \overline{BI} \rangle$ for wandering and braided rivers ($R^2 = 0.75$; RMSE = 0.04; Figure 11b). For both braided and wandering rivers, Q^* exerts the greatest influence on floodplain reworking timescale, with spatial configuration and its changes—quantified by $\langle \overline{eBI} \rangle$ and standard deviation of $\overline{eBI}$—playing a secondary role ($R^2 = 0.25$; RMSE = 10.94; Figure 11c). At the channel-belt scale, floodplain reworking timescale is a key predictor of normalized channel-belt area in wandering rivers ($R^2 = 0.21$; RMSE = 2.09 for braided; $R^2 = 0.27$; RMSE = 5.69 for wandering; Figure 11d), while Q^* more strongly predicts this metric in braided rivers.

4. Discussion

4.1. Comparing Dynamics Across Planform Morphologies

Our results demonstrate both striking quantitative similarities and differences between wandering and braided rivers—often considered distinct classes of multithread rivers (e.g., Galeazzi et al., 2021). Traditional classifications of multithread rivers (i.e., wandering, braided, anastomosing, and anabranching) rely on static snapshots, neglecting temporal dynamics (Galeazzi et al., 2021). We observed rivers transitioning between wandering and braided classifications at both cross-sectional and reach scales over time (Figures 4j–4l), highlighting the temporal variability of multithread rivers and emphasizing the need for more quantitative planform descriptors that incorporate river dynamics. We find that both planform types exhibit increased thread counts with increasing discharge (Figure 5a), consistent with previous experimental work (Ashmore, 2009; Egozi & Ashmore, 2009). We also find that both river types partition flow between threads similarly, despite their differences in active thread count (Figure 5). Despite the similarities in how the kinematics of braided rivers and wandering rivers respond to discharge variations (Figure 5a), we find that braided rivers, though represented by fewer observations, plot as separate populations in how their spatial configuration responds to discharge variation. Specifically, thread counts in braided rivers show a stronger sensitivity to variations in water discharge than wandering rivers (Figure 5a). Although braided rivers are generally considered "flashier," we find that flow intermittency does not differ significantly between braided and wandering rivers.

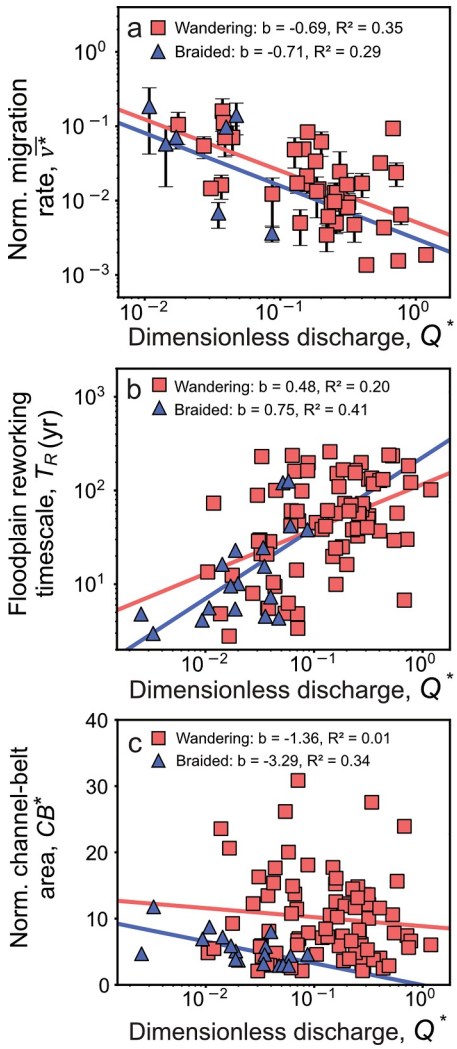

Figure 9. Functional dependence of (a) normalized riverbank migration rate (data shown on log-log axes), (b) floodplain reworking timescale (data shown on log-log axes), and (c) normalized channel-belt area on dimensionless discharge (data shown on semi-log axes). Blue triangles and red squares denote braided and wandering rivers, respectively. The fitted equation in panels (a, b) are given by $y = ax^b$, and the equation in panel (c) is $y = a + b$*log x. See Text S2 in Supporting Information S1 for details on fitted equations.

4.2. The Relative Importance of Mean Flows, Flow Intermittency, and Flow Partitioning

Our results demonstrate that the dimensionless discharge, Q^* (ratio of long-term water discharge and an estimate of bankfull discharge; Equation 3), exerts a primary control on the spatial configuration and kinematic evolution of multithread rivers. Similar to mean discharge, we find that $\langle \overline{eBI} \rangle$ increases with Q^* for both river types, but more sharply in braided rivers (Figure 4b). In addition, our random forest regression model identifies Q^* as a key predictor of $\langle \overline{eBI} \rangle$ in both channel patterns (Figure 11a). We also find that Q^* is a key predictor of kinematic changes of multithread rivers across the bank, reach, and belt scales (Figure 11). With increasing dimensionless discharge, normalized bank migration rates decline (Figure 9a), the floodplain reworking timescales increase (Figure 9b), and the normalized channel-belt area decreases across all multithread rivers (Figure 9c). However, we did not find a similar trend between mean discharge and the kinematic changes of multithread rivers (Figure S4 in Supporting Information S1) indicating that it is the dimensionless discharge, and not the mean discharge, that likely exerts the primary control on multithread river evolution.

We interpret the dimensionless discharge, commonly used in previous studies that employ median grain size as the characteristic length scale for renormalization (Métivier et al., 2017), as a proxy for river flow intermittency (Text S1 in Supporting Information S1). Specifically, low Q^* values correspond to highly intermittent flows, where the mean discharge is significantly less than the bankfull capacity. Conversely, higher Q^* values reflect more perennial conditions, with mean water discharge approaching or exceeding bankfull capacity (Figure S1 in Supporting Information S1). While both Q_{cov} and Q^* describe aspects of flow variability, Q^* expresses this variability in the context of channel morphology. Our analyses reveal that Q^* consistently ranks as a strong predictor of spatial configuration and dynamics of multithread rivers in our random forest regression analyses (Figure 11), when compared to Q_{cov}. Moreover, we find that Q^* can vary widely for a given Q_{cov} (Figure S5a in Supporting Information S1), indicating that these measures need not covary closely. Notably, within a given range of Q_{cov}, river mobility —quantified by T_R—shows a strong trend with Q^* in wandering and braided rivers (Figure S5b in Supporting Information S1). This suggests that normalizing discharge by a characteristic channel scale, rather than just variability alone, provides a more mechanistic foundation for predicting multithread river evolution.

Our implementation of *eBI* enables us to quantify how multithread rivers partition flow among individual threads. We show that preferential flow routing emerges primarily at higher discharges and lower slopes, a pattern observed consistently in both braided and wandering rivers (Figure 4). Larger rivers systematically exhibit stronger preferential flow routing, directing water into one or a few dominant threads. Furthermore, dimensionless discharge regulates flow partitioning: highly intermittent rivers (low Q^*) distribute flow more evenly across multiple threads, while less intermittent rivers favor a dominant thread (high Q^*; Figure 5b). Our random forest regression analysis identifies Q^* as the foremost predictor for preferential flow routing into individual threads (Figure 11b). We observe similar relationships between Q_{mean} and Q^* with $\langle \overline{eBI} \rangle$ and $\langle \overline{eBI} \rangle / \langle \overline{BI} \rangle$ (Figures 5 and 6) likely because all of reaches exceed 200 m in width and thus buffer small-scale fluctuations in water discharge. In narrower rivers, changes in water discharge might exert a larger influence on channel geometry.

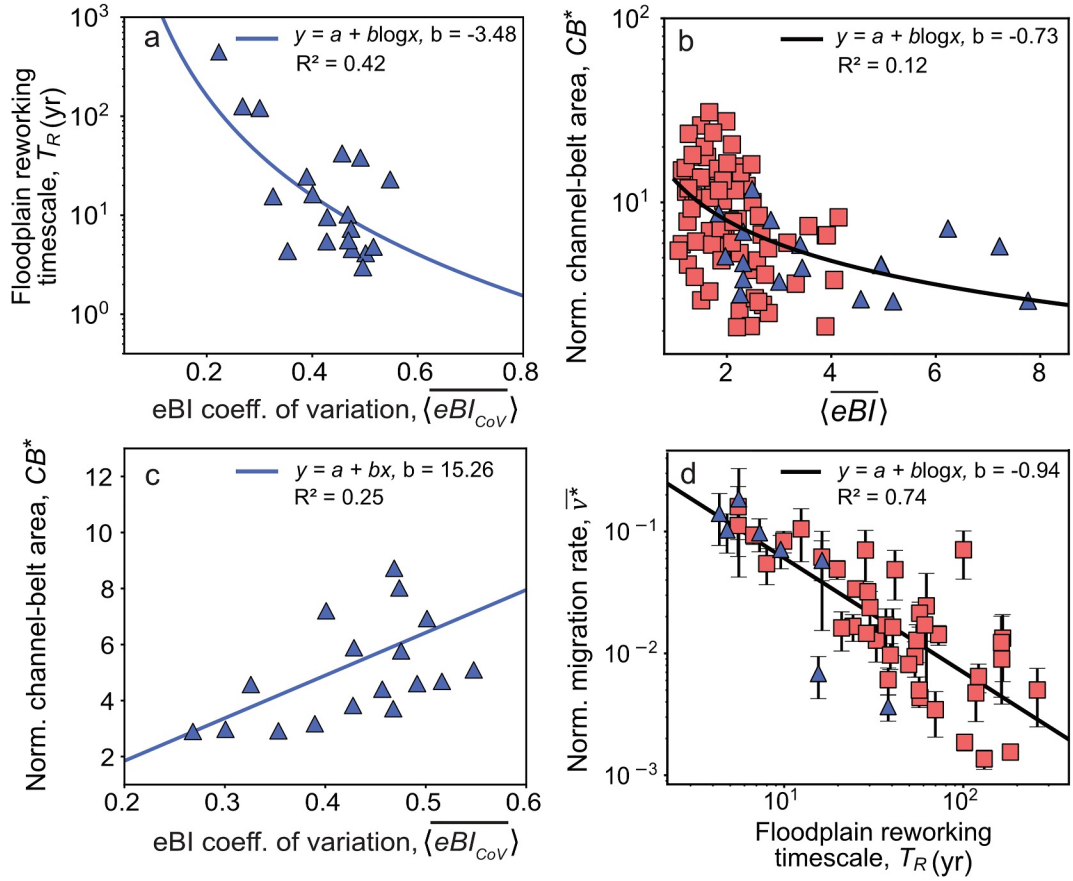

Figure 10. (a) Relationship between coefficient of variation of temporal changes in reach-averaged entropic braiding index and floodplain reworking timescale. Only braided rivers exhibit a negative relationship. Data are shown on semi-log axes. (b) Relationship between reach- and time-averaged value of entropic braiding index and normalized channel-belt area. (c) Relationship between coefficient of variation of *eBI* through time and normalized channel-belt area. Only braided rivers exhibit a positive relationship. (d) Relationship between floodplain reworking timescale and normalized migration rate. Blue triangles denote braided rivers, and red squares denote wandering rivers. See Text S2 in Supporting Information S1 for details on fitted equations.

4.3. Assumptions and Limitations

Sample sizes for braided rivers are smaller than for wandering rivers (n = 8–18 depending on migration-rate availability), which could in principle introduce sample-size bias. Bootstrap resampling analyses (Text S3 in Supporting Information S1) indicate that the direction of key trends for braided rivers remains robust, although parameter estimates show increased uncertainty. Where direct comparison is possible, braided rivers follow the same directional trends as wandering rivers, differing primarily in magnitude.

We also recognize that Q^* and $\langle \overline{eBI} \rangle$ both incorporate the traditional braiding index (*BI*), which raises the possibility that their correlation could partly reflect shared-variable structure rather than fully independent processes. However, *BI* enters these quantities through distinct physical roles: in *eBI*, *BI* reflects the number of threads, whereas in Q^* it appears within a hydraulic scaling that reflects discharge partitioning, channel width, and mass conservation. Similar shared-variable dependencies commonly arise in hydraulic geometry analyses and do not, by themselves, imply spurious correlation when those relationships follow from well-defined physical constraints (Parker et al., 2007).

4.4. Implications for River Response to Environmental Change

Our work provides a comprehensive view of multithread river dynamics. We find that rivers in cold climate zones display slower bank migration rates, floodplain reworking, and smaller channel belts—aligning with

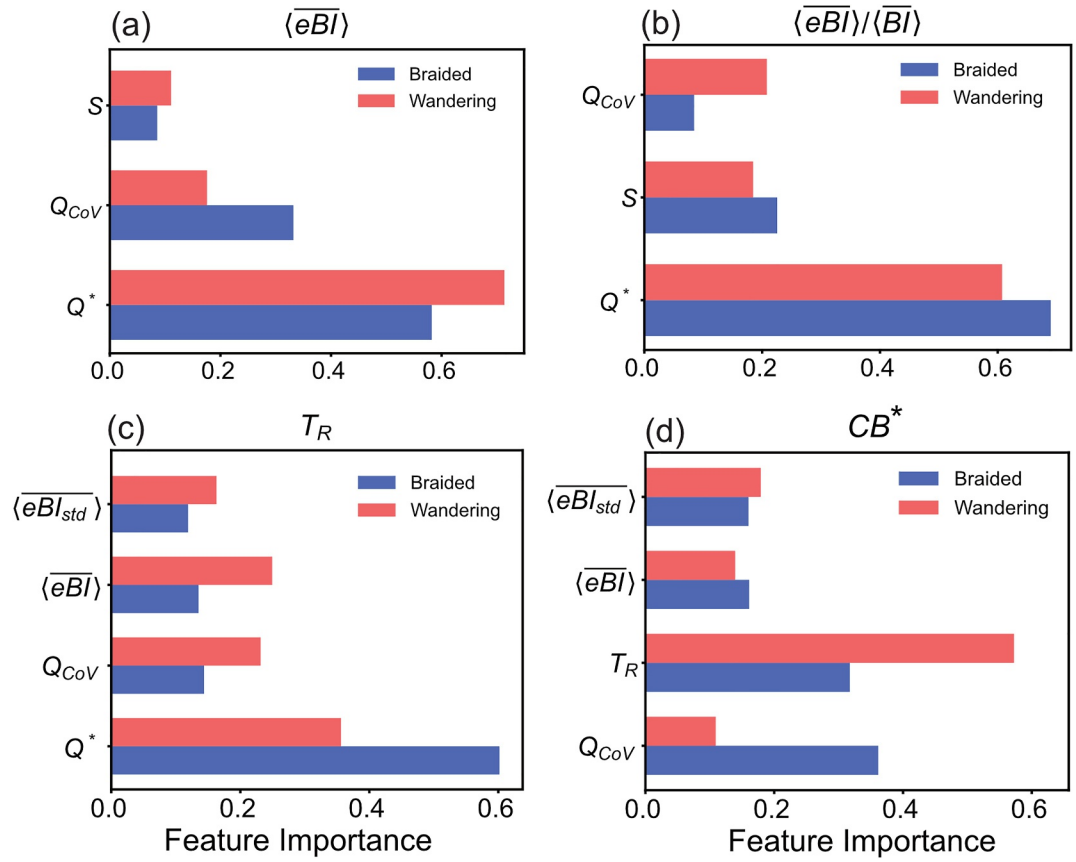

Figure 11. Random forest analysis reveals the primary controls on multithread river evolution. (a) Feature importance of the best predictors for the time- and reach-averaged entropic Braiding Index ($\langle \overline{eBI} \rangle$) of braided and wandering rivers. Similar plots showing the feature importance in random forest regression model for predicting the (b) ratio of entropic Braiding Index to Braiding Index ($\langle \overline{eBI} \rangle / \langle \overline{BI} \rangle$), (c) floodplain reworking timescale (T_R), and (d) normalized channel-belt area (CB^*). Predictor variables include dimensionless discharge (Q^*), coefficient of variation of water discharge (Q_{CoV}), channel slope (S), and *eBI* variability ($\langle \overline{eBI}_{std} \rangle$). Feature importance is expressed as the mean decrease in impurity across 500 trees.

previous studies (Ielpi et al., 2023; Geyman et al., 2024; Figure 7). This observation supports the hypothesis that permafrost presence and seasonal river ice slows kinematic evolution of rivers over annual to multi-decadal timescales (Geyman et al., 2024; Rowland et al., 2010, 2023). Seasonal ice cover and reduced open-water duration will likely decrease discharge and bank erosion, reinforcing slower channel migration in cold environments (Geyman et al., 2024). A warming climate may accelerate the evolution of these rivers by weakening permafrost and altering ice-breakup dynamics, potentially affecting organic carbon storage in river corridors (Geyman et al., 2025). Furthermore, we observed a link between Q^* and riverbank migration rates across all multithread rivers. We interpret this trend to imply that highly intermittent flows are associated with faster normalized bank migration rates (Figure 9a), suggesting intense bankfull-overtopping floods drive larger bank migration in braided and wandering rivers (Inoue et al., 2025). On decadal and millennial timescales, significant differences in river mobility emerge between braided and wandering rivers. Braided rivers exhibit faster thread migration and floodplain reworking despite forming smaller normalized channel belts (Figures 8d and 10b). This seemingly counterintuitive result stems from the rapid spatial reconfiguration within braided rivers, which confines active channel migration to narrower bounds, effectively accelerating sediment export (Greenberg et al., 2024).

The observed sensitivity of multithread rivers to prevailing hydroclimate—mean discharge and variability—has important implications under future climate scenarios. Increased global runoff, particularly in high-altitude areas, may amplify active thread counts, especially in braided rivers (Figure 5a; Li et al., 2021, 2022). Heightened flow intermittency could lead to more even flow partitioning among threads (Figure 5), significantly influencing flow

patterns and associated hydrological conditions globally (Immerzeel et al., 2010). Our global analysis provides a crucial baseline for how multithread rivers respond to variations in water discharge, informing mechanistic predictions of their response to climate change and human interference.

5. Conclusions

Our analysis of 97 river reaches provides a quantitative framework for understanding the key controls on multithread river evolution, revealing how these complex systems respond to environmental drivers. Our results demonstrate.

1. Thread count scales with discharge: both wandering and braided rivers exhibit increased thread count with increasing mean and dimensionless water discharge (Figure 6).
2. Hydrologic regime controls flow partitioning in multithread rivers: large, low-gradient rivers with perennial flows concentrate flow into dominant threads, while highly intermittent flows promote the even distribution of flow among all active threads (Figure 5).
3. Permafrost slows river evolution across scales: multithread rivers in cold climates evolve at slower rates—evidenced by reduced bank migration, longer floodplain reworking timescales, and smaller normalized channel-belt sizes—likely due to permafrost influence (Geyman et al., 2024; Ielpi et al., 2023; Kanevskiy et al., 2016).
4. Braided rivers rapidly rework floodplains through both spatial reconfiguration and lateral migration, while wandering rivers primarily rework floodplain through lateral migration.
5. Thread count constrains channel-belt size: across all rivers, channel-belt area normalized by channelized area declines exponentially with active thread count. This trend could indicate that distinct dynamics shape floodplain development in braided and wandering rivers, with the former characterized by both lateral migration and pronounced spatial configuration changes and the latter primarily laterally migrate.

These findings provide critical insights into how multithread rivers respond to changing hydrological regimes, providing crucial information for predicting future river behavior in a world facing increasing runoff and flow variability.

Notation

eBI	cross-sectional entropic braiding index
BI	cross-sectional braiding index
$\overline{eBI}$	reach-averaged entropic braiding index
$\overline{BI}$	reach-averaged braiding index
$\langle\overline{eBI}\rangle$	time- and reach-averaged entropic braiding index
$\langle\overline{BI}\rangle$	time- and reach-averaged braiding index
$\langle\overline{eBI_{\text{std}}}\rangle$	standard deviation of reach-averaged eBI
$\langle\overline{eBI_{\text{cov}}}\rangle$	coefficient of variation of reach-averaged eBI
$\overline{eBI}/\overline{BI}$	ratio of reach-averaged eBI to BI
$\langle\overline{eBI}\rangle/\langle\overline{BI}\rangle$	ratio of time- and reach-averaged eBI to BI
Q^*	dimensionless water discharge (Equation 3)
Q_{mean}	mean water discharge (m^3/s)
Q_{cov}	coefficient of variation of water discharge
S	riverbed slope
T_R	floodplain reworking timescale (years)
$\overline{\nu^*}$	normalized bank migration rate (1/year)

$\overline{v}$	mean bank migration rate (m/year)
CB^*	normalized channel belt size

Conflict of Interest

The authors declare no conflicts of interest relevant to this study.

Availability Statement

The data and code underlying this study are publicly available on the Dryad repository (Zhao et al., 2026). Our analysis was performed using Google Earth Engine (Gorelick et al., 2017) and Python 3 (van Rossum & Drake, 1995). Codes to run Rivgraph can be downloaded at Schwenk & Hariharan, 2021.

Acknowledgments
We thank Alejandro Tejedor for useful discussions, as well as Tian Dong and two anonymous reviewers for their constructive feedback. This work is supported by National Science Foundation (EAR2310740) and NASA (80NSSC24K0046) Grants to V.G., and the National Science Foundation (GAIG-425748, EAR-2342937, and IIS-2324008) grants and the Samueli Endowed Chair to EF-G.

References

Ashmore, P. (2009). Intensity and characteristic length of braided channel patterns. *Canadian Journal of Civil Engineering*, *36*(10), 1656–1666. https://doi.org/10.1139/L09-088

Ashmore, P., Bertoldi, W., & Tobias Gardner, J. (2011). Active width of gravel-bed braided rivers. *Earth Surface Processes and Landforms*, *36*(11), 1510–1521. https://doi.org/10.1002/esp.2182

Bertoldi, W., Tubino, M., & Ashmore, P. (2008). Bed load evaluation in gravel-bed braided streams. In *Proceedings of the International Conference on Fluvial Hydraulics* (Vol. 2, pp. 1331–1338). KUBABA Congress Department and Travel Services.

Bertoldi, W., Zanoni, L., & Tubino, M. (2009). Planform dynamics of braided streams. *Earth Surface Processes and Landforms*, *34*(4), 547–557. https://doi.org/10.1002/esp.1755

Best, J. (2019). Anthropogenic stresses on the world's big rivers. *Nature Geoscience*, *12*(1), 7–21. https://doi.org/10.1038/s41561-018-0262-x

Bridge, J. S. (1985). Paleochannel patterns inferred from alluvial deposits: A critical evaluation. *Journal of Sedimentary Petrology*, *55*(4), 579–589. https://doi.org/10.1306/212F8738-2B24-11D7-8648000102C1865D

Brooke, S., Chadwick, A. J., Silvestre, J., Lamb, M. P., Edmonds, D. A., & Ganti, V. (2022). Where rivers jump course. *Science*, *376*(6596), 987–990. https://doi.org/10.1126/science.abm1215

Carling, P., Jansen, J., & Meshkova, L. (2014). Multichannel rivers: Their definition and classification. *Earth Surface Processes and Landforms*, *39*(1), 26–37. https://doi.org/10.1002/esp.3419

Chadwick, A. J., Greenberg, E., & Ganti, V. (2023). Remote sensing of riverbank migration using particle image velocimetry. *Journal of Geophysical Research: Earth Surface*, *128*(7), e2023JF007177. https://doi.org/10.1029/2023JF007177

Chadwick, A. J., Greenberg, E., & Ganti, V. (2025). Single-and multithread rivers originate from (im) balance between lateral erosion and accretion. *Science*, *389*(6756), 146–150. https://doi.org/10.1126/science.ads6567

Church, M., & Ferguson, R. I. (2015). Morphodynamics: Rivers beyond steady state. *Water Resources Research*, *51*(4), 1883–1897. https://doi.org/10.1002/2014WR016862

Constantine, J. A., Dunne, T., Ahmed, J., Legleiter, C., & Lazarus, E. D. (2014). Sediment supply as a driver of river meandering and floodplain evolution in the Amazon Basin. *Nature Geoscience*, *7*(12), 899–903. Article 12. https://doi.org/10.1038/ngeo2282

Dethier, E. N., Renshaw, C. E., & Magilligan, F. J. (2022). Rapid changes to global river suspended sediment flux by humans. *Science*, *376*(6600), 1447–1452. https://doi.org/10.1126/science.abn7980

Dong, T. Y., & Goudge, T. A. (2022). Quantitative relationships between river and channel-belt planform patterns. *Geology*, *50*(9), 1053–1057. https://doi.org/10.1130/G49935.1

Dong, T. Y., Nittrouer, J. A., McElroy, B., Il'icheva, E., Pavlov, M., Ma, H., et al. (2020). Predicting water and sediment partitioning in a delta channel network under varying discharge conditions. *Water Resources Research*, *56*(11), e2020WR027199. https://doi.org/10.1029/2020WR027199

Dunne, K. B., & Jerolmack, D. J. (2018). Evidence of, and a proposed explanation for, bimodal transport states in alluvial rivers. *Earth Surface Dynamics*, *6*(3), 583–594. https://doi.org/10.5194/esurf-6-583-2018

Eaton, B. C., Millar, R. G., & Davidson, S. (2010). Channel patterns: Braided, anabranching, and single-thread. *Geomorphology*, *120*(3–4), 353–364. https://doi.org/10.1016/j.geomorph.2010.04.010

Egozi, R., & Ashmore, P. (2008). Defining and measuring braiding intensity. *Earth Surface Processes and Landforms*, *33*(14), 2121–2138. https://doi.org/10.1002/esp.1658

Egozi, R., & Ashmore, P. (2009). Experimental analysis of braided channel pattern response to increased discharge. *Journal of Geophysical Research*, *114*(F2). https://doi.org/10.1029/2008JF001099

Ethridge, F. G. (2011). Interpretation of ancient fluvial channel deposits: Review and recommendations. https://doi.org/10.2110/sepmsp.097.009

Galeazzi, C. P., Almeida, R. P. D., & Do Prado, A. H. (2021). Linking rivers to the rock record: Channel patterns and paleocurrent circular variance. *Geology*, *49*(11), 1402–1407. https://doi.org/10.1130/G49121.1

Geyman, E. C., Douglas, M. M., Avouac, J. P., & Lamb, M. P. (2024). Permafrost slows Arctic riverbank erosion. *Nature*, *634*(8033), 359–365. https://doi.org/10.1038/s41586-024-07978-w

Geyman, E. C., Ke, Y., Magyar, J. S., Reahl, J. N., Soldano, V., Brown, N. D., et al. (2025). Scaling laws for sediment storage and turnover in river floodplains. *Science Advances*, *11*(15), eadu8574. https://doi.org/10.1126/sciadv.adu8574

Gorelick, N., Hancher, M., Dixon, M., Ilyushchenko, S., Thau, D., & Moore, R. (2017). Google Earth Engine: Planetary-scale geospatial analysis for everyone. *Remote Sensing of Environment*, *202*, 18–27. https://doi.org/10.1016/j.rse.2017.06.031

Greenberg, E., Chadwick, A. J., & Ganti, V. (2023). A generalized area-based framework to quantify river mobility from remotely sensed imagery. *Journal of Geophysical Research: Earth Surface*, *128*(9), e2023JF007189. https://doi.org/10.1029/2023JF007189

Greenberg, E., Chadwick, A. J., Li, G. K., & Ganti, V. (2024). Quantifying channel mobility and floodplain reworking timescales across river planform morphologies. *Geophysical Research Letters*, *51*(12), e2024GL108537. https://doi.org/10.1029/2024GL108537

Greenberg, E., & Ganti, V. (2024). The pace of global river meandering influenced by fluvial sediment supply. *Earth and Planetary Science Letters*, *634*, 118674. https://doi.org/10.1016/j.epsl.2024.118674

Greenberg, E., Ganti, V., & Hajek, E. (2021). Quantifying bankfull flow width using preserved bar clinoforms from fluvial strata. *Geology*, *49*(9), 1038–1043. https://doi.org/10.1130/G48729

Hansford, M. R., Plink-Björklund, P., & Jones, E. R. (2020). Global quantitative analyses of river discharge variability and hydrograph shape with respect to climate types. *Earth-Science Reviews*, *200*, 102977. https://doi.org/10.1016/j.earscirev.2019.102977

Hasson, M., Finotello, A., Ielpi, A., & Lapôtre, M. G. A. (2025). Vegetation changes the trajectory of river bends. *Science*, *389*(6763), 915–920. https://doi.org/10.1126/science.adv4939

Hickin, E. J., & Nanson, G. C. (1984). Lateral migration rates of river bends. *Journal of Hydraulic Engineering*, *110*(11), 1557–1567. https://doi.org/10.1061/(ASCE)0733-9429(1984)110:11(1557)

Hooke, J. (2003). River meander behaviour and instability: A framework for analysis. *Transactions of the Institute of British Geographers*, *28*(2), 238–253. https://doi.org/10.1111/1475-5661.00089

Howard, A. D. (1996). Modeling channel evolution and floodplain morphology. *Floodplain processes*, 15–62.

Huang, H. Q., & Nanson, G. C. (2007). Why some alluvial rivers develop an anabranching pattern. *Water Resources Research*, *43*(7). https://doi.org/10.1029/2006WR005223

Ielpi, A., & Lapôtre, M. G. (2020). A tenfold slowdown in river meander migration driven by plant life. *Nature Geoscience*, *13*(1), 82–86. https://doi.org/10.1038/s41561-019-0491-7

Ielpi, A., & Lapôtre, M. G. (2022). Linking sediment flux to river migration in arid landscapes through mass balance. *Journal of Sedimentary Research*, *92*(8), 695–703. https://doi.org/10.2110/jsr.2022.118

Ielpi, A., Lapôtre, M. G., Finotello, A., & Roy-Léveillée, P. (2023). Large sinuous rivers are slowing down in a warming Arctic. *Nature Climate Change*, *13*(4), 375–381. https://doi.org/10.1038/s41558-023-01620-9

Immerzeel, W. W., Van Beek, L. P., & Bierkens, M. F. (2010). Climate change will affect the Asian water towers. *Science*, *328*(5984), 1382–1385. https://doi.org/10.1126/science.1183188

Inoue, T., Hiramatsu, Y., Johnson, J. P. L., Dempo, J., & Mishra, J. (2025). Ratio of river channel bar to bank height sets bank erosion rate. *Journal of Geophysical Research: Earth Surface*, *130*(1), e2024JF007965. https://doi.org/10.1029/2024JF007965

Jerolmack, D. J. (2009). Conceptual framework for assessing the response of delta channel networks to Holocene sea level rise. *Quaternary Science Reviews*, *28*(17), 1786–1800. https://doi.org/10.1016/j.quascirev.2009.02.015

Jones, J. W. (2019). Improved automated detection of subpixel-scale inundation—Revised Dynamic Surface Water Extent (DSWE) partial surface water tests. *Remote Sensing*, *11*(4), 374. Article 4. https://doi.org/10.3390/rs11040374

Kanevskiy, M., Shur, Y., Strauss, J., Jorgenson, T., Fortier, D., Stephani, E., & Vasiliev, A. (2016). Patterns and rates of riverbank erosion involving ice-rich permafrost (yedoma) in northern Alaska. *Geomorphology*, *253*, 370–384. https://doi.org/10.1016/j.geomorph.2015.10.023

Kleinhans, M. G., & van den Berg, J. H. (2011). River channel and bar patterns explained and predicted by an empirical and a physics-based method. *Earth Surface Processes and Landforms*, *36*(6), 721–738. https://doi.org/10.1002/esp.2090

Kottek, M., Grieser, J., Beck, C., Rudolf, B., & Rubel, F. (2006). World map of the Köppen-Geiger climate classification updated. https://doi.org/10.1127/0941-2948/2006/0130

Latrubesse, E. M. (2008). Patterns of anabranching channels: The ultimate end-member adjustment of Mega Rivers. *Geomorphology*, *101*(1), 130–145. https://doi.org/10.1016/j.geomorph.2008.05.035

Leenman, A., Greenberg, E., Moulds, S., Wortmann, M., Slater, L., & Ganti, V. (2025). Accelerated river mobility linked to water discharge variability. *Geophysical Research Letters*, *52*(2), e2024GL112899. https://doi.org/10.1029/2024GL112899

Leopold, L. B., & Wolman, M. G. (1957). *River flood plains: Some observations on their formation (No. 282-C)* (pp. 87–109). US Government Printing Office. https://doi.org/10.3133/pp282C

Li, D., Lu, X., Walling, D. E., Zhang, T., Steiner, J. F., Wasson, R. J., et al. (2022). High Mountain Asia hydropower systems threatened by climate-driven landscape instability. *Nature Geoscience*, *15*(7), 520–530. https://doi.org/10.1038/s41561-022-00953-y

Li, D., Lu, X. X., Overeem, I., Walling, D. E., Syvitski, J., Kettner, A. J., et al. (2021). Exceptional increases in fluvial sediment fluxes in a warmer and wetter High Mountain Asia. *Science*, *374*(6567), 599–603. https://doi.org/10.1126/science.abi9649

Limaye, A. B. (2017). Extraction of multithread channel networks with a reduced-complexity flow model. *Journal of Geophysical Research: Earth Surface*, *122*(10), 1972–1990. https://doi.org/10.1002/2016JF004175

Limaye, A. B. (2020). How do braided rivers grow channel belts? *Journal of Geophysical Research: Earth Surface*, *125*(8), e2020JF005570. https://doi.org/10.1029/2020JF005570

Limaye, A. B., Grimaud, J.-L., Lai, S. Y. J., Foreman, B. Z., Komatsu, Y., & Paola, C. (2018). Geometry and dynamics of braided channels and bars under experimental density currents. *Sedimentology*, *65*(6), 1947–1972. https://doi.org/10.1111/sed.12453

Mason, J., & Mohrig, D. (2019). Differential bank migration and the maintenance of channel width in meandering river bends. *Geology*, *47*(12), 1136–1140. https://doi.org/10.1130/G46651.1

Métivier, F., Lajeunesse, E., & Devauchelle, O. (2017). Laboratory rivers: Lacey's law, threshold theory, and channel stability. *Earth Surface Dynamics*, *5*(1), 187–198. https://doi.org/10.5194/esurf-5-187-2017

Miall, A. D. (1994). Reconstructing fluvial macroform architecture from two-dimensional outcrops: Examples from the Castlegate Sandstone, Book Cliffs, Utah. *Journal of Sedimentary Research*, *64*(2B), 146–158. https://doi.org/10.1306/d4267f78-2b26-11d7-8648000102c1865d

Miall, A. D. (2014). *Fluvial depositional systems*. Springer. https://doi.org/10.1007/978-3-319-00666-6_5

Mosley, M. P. (1983). Response of braided Rivers to changing discharge. *Journal of Hydrology*, *22*(1), 18–67.

NASA JPL. (2020). NASADEM merged DEM global 1arcsecond V001 [Dataset]. *NASA*. https://doi.org/10.5067/MEASURES/NASADEM/NASADEM_HGT.001

Nicholas, A. P. (2013). Modelling the continuum of river channel patterns. *Earth Surface Processes and Landforms*, *38*(10), 1187–1196. https://doi.org/10.1002/esp.3431

Nyberg, B., Henstra, G., Gawthorpe, R. L., Ravnås, R., & Ahokas, J. (2023). Global scale analysis on the extent of river channel belts. *Nature Communications*, *14*(1), 2163. https://doi.org/10.1038/s41467-023-37852-8

Parker, G., Wilcock, P. R., Paola, C., Dietrich, W. E., & Pitlick, J. (2007). Physical basis for quasi-universal relations describing bankfull hydraulic geometry of single-thread gravel bed rivers. *Journal of Geophysical Research*, *112*(F4). https://doi.org/10.1029/2006JF000549

Repasch, M., Scheingross, J. S., Hovius, N., Lupker, M., Wittmann, H., Haghipour, N., et al. (2021). Fluvial organic carbon cycling regulated by sediment transit time and mineral protection. *Nature Geoscience*, *14*(11), 842–848. https://doi.org/10.1038/s41561-021-00845-7

Rowland, J. C., Jones, C. E., Altmann, G., Bryan, R., Crosby, B. T., Geernaert, G. L., et al. (2010). Arctic landscapes in transition: Responses to thawing permafrost. *Eos, Transactions American Geophysical Union*, *91*(26), 229–236. https://doi.org/10.1029/2010EO260001

Rowland, J. C., Schwenk, J. P., Shelef, E., Muss, J., Ahrens, D., Stauffer, S., et al. (2023). Scale-dependent influence of permafrost on riverbank erosion rates. *Journal of Geophysical Research: Earth Surface*, *128*(7), e2023JF007101. https://doi.org/10.1029/2023JF007101

Salo, J., Kalliola, R., Häkkinen, I., Mäkinen, Y., Niemelä, P., Puhakka, M., & Coley, P. D. (1986). River dynamics and the diversity of Amazon lowland forest. *Nature*, *322*(6076), 254–258. https://doi.org/10.1038/322254a0

Sapozhnikov, V. B., & Foufoula-Georgiou, E. (1997). Experimental evidence of dynamic scaling and indications of self-organized criticality in braided rivers. *Water Resources Research*, *33*(8), 1983–1991. https://doi.org/10.1029/97WR01233

Sapozhnikov, V. B., Murray, A. B., Paola, C., & Foufoula-Georgiou, E. (1998). Validation of braided-stream models: Spatial state-space plots, self-affine scaling, and island shapes. *Water Resources Research*, *34*(9), 2353–2364. https://doi.org/10.1029/98WR01697

Schwenk, J., & Hariharan, J. (2021). RivGraph: Automatic extraction and analysis of river and delta channel network topology. *Journal of Open Source Software*, *6*(59), 2952. Article LA-UR-21-20218. https://doi.org/10.21105/joss.02952

Schwenk, J., Piliouras, A., & Rowland, J. C. (2020). Determining flow directions in river channel networks using planform morphology and topology. *Earth Surface Dynamics*, *8*(1), 87–102. https://doi.org/10.5194/esurf-8-87-2020

Slater, L. J., & Singer, M. B. (2013). Imprint of climate and climate change in alluvial riverbeds: Continental United States, 1950–2011. *Geology*, *41*(5), 595–598. https://doi.org/10.1130/G34070.1

Slingerland, R., & Smith, N. D. (2004). River avulsions and their deposits. *Annual Review of Earth and Planetary Sciences*, *32*(1), 257–285. https://doi.org/10.1146/annurev.earth.32.101802.120201

Sylvester, Z., Durkin, P., & Covault, J. A. (2019). High curvatures drive river meandering. *Geology*, *47*(3), 263–266. https://doi.org/10.1130/G45608.1

Tejedor, A., Schwenk, J., Kleinhans, M., Limaye, A. B., Vulis, L., Carling, P., et al. (2022). The Entropic Braiding Index (*eBI*): A robust metric to account for the diversity of channel scales in multi-thread rivers. *Geophysical Research Letters*, *49*(16), e2022GL099681. https://doi.org/10.1029/2022GL099681

Thakur, P. K., Laha, C., & Aggarwal, S. P. (2012). River bank erosion hazard study of river Ganga, upstream of Farakka barrage using remote sensing and GIS. *Natural Hazards*, *61*(3), 967–987. https://doi.org/10.1007/s11069-011-9944-z

Torres, M. A., Limaye, A. B., Ganti, V., Lamb, M. P., West, A. J., & Fischer, W. W. (2017). Model predictions of long-lived storage of organic carbon in river deposits. *Earth Surface Dynamics*, *5*(4), 711–730. https://doi.org/10.5194/esurf-2017-29

Tucker, C. J. (1979). Red and photographic infrared linear combinations for monitoring vegetation. *Remote Sensing of Environment*, *8*(2), 127–150. https://doi.org/10.1016/0034-4257(79)90013-0

Valenza, J. M., Edmonds, D. A., Hwang, T., & Roy, S. (2020). Downstream changes in river avulsion style are related to channel morphology. *Nature Communications*, *11*(1), 2116. https://doi.org/10.1038/s41467-020-15859-9

van Rossum, G., & Drake, F. L., Jr. (1995). Python reference manual. *Centrum voor Wiskunde en Informatica*.

Wang, B., & Smith, L. C. (2025). Remote sensing of discharge ratios at river channel bifurcations. *Geophysical Research Letters*, *52*(8), e2024GL114045. https://doi.org/10.1029/2024GL114045

Zarrabi, R., McDermott, R., Erfani, S. M. H., & Cohen, S. (2025). Bankfull and mean-flow channel geometry estimation through machine learning algorithms across the contiguous United States (CONUS). *Water Resources Research*, *61*(2), e2024WR037997. https://doi.org/10.1029/2024WR037997

Zhao, F., Ganti, V., Chadwick, A., Greenberg, E., McLeod, J., Liu, Y., et al. (2026). Global hydroclimatic controls on multithread river dynamics [Dataset]. *Dryad*. https://doi.org/10.5061/dryad.tx95x6b9s

Zhao, F., Ganti, V., & Limaye, A. B. (2024). Scour-depth variability controls channel-scale stratigraphy in experimental braided rivers. *Journal of Sedimentary Research*, *94*(3), 302–312. https://doi.org/10.2110/jsr.2023.118

References From the Supporting Information

Liu, Y., Wortmann, M., & Slater, L. (2025). Global River BankFull Discharge (GQBF)—Coefficient of variation (0.1) [Dataset]. *Zenodo*. https://doi.org/10.5281/zenodo.17456624